Laminar analysis of the slow wave activity in humans

Doctoral thesis

Csercsa Richárd

Semmelweis University
János Szentágothai School of Neurosciences

Supervisor: Dr. Ulbert István Ph.D.

Official opponents: Dr. Anita Kamondi C.Sc.
Dr. Péter Barthó Ph.D.

President of committee: Dr. Imre Szirmai Ph.D., D.Sc.
Members of committee: Dr. Róbert Bódizs Ph.D.
Dr. Viktor Gál Ph.D.

Budapest
2010

Introduction

The fundamental mode of operation of the brain is through oscillations. They are thought to determine cortical excitability, hence the way of information processing. They are traditionally divided into several frequency bands, with different bands assigned to different functions. A fundamental oscillation in mammalian cortex is the slow (<1Hz) oscillation (SO) during the deepest stage of non-rapid eye movement (NREM) sleep. In humans, this stage (the third and deepest stage of NREM sleep; N3, also called slow wave sleep; SWS) is accompanied by big amplitude waves of slow wave activity (SWA, 0.5-2 Hz) in the frontal EEG, and the behavioural signs of sleep. Delta waves (0-4 Hz) during sleep were reported in 1937, but slow oscillations, the main characteristic electrophysiological features of deep sleep were first described by Mircea Steriade in 1993 in anesthetized cats. Intracellular recordings have revealed that SO are composed of rhythmically alternating phases of increased cellular and synaptic activity (up-states) and hyperpolarisation accompanied by cellular silence (down-states). In humans, the alpha and beta spectral components during the surface positive SWA half-wave (up-state) are increased compared to the surface negative SWA half-wave (down-state), suggesting that their basic neurophysiology may be similar to animal findings. While the SO in animals is traditionally restrained to below 1 Hz, the recent American Academy of Sleep Medicine (AASM) guidelines suggest the 0.5-2 Hz range for SWA in humans.

Slow waves are thought to underlie restorative sleep functions and serve memory consolidation via ensemble reactivation and synaptic strength normalization. They might play an important role in the transfer of memory traces from hippocampus to neocortex.

SO can be induced artificially by various anaesthetics in vivo, and ionic environments in vitro. SO are traditionally considered to be generated in neocortical networks, since it is present in the neocortex after thalamectomy, but absent in the thalamus after decortications, and the disconnection of intracortical synaptic linkages results in the disruption of its long-range synchronization. However, Crunelli and his colleagues recently suggested a complex thalamo-cortical interplay in SO generation.

Current source density (CSD) analysis, showing the local trans-membrane currents, localized the most prominent up-state related sinks to the middle and deepest cortical layers (most probably layer III-VI) in anesthetized cats. In the rat primary auditory cortex, the laminar distribution of the major sink during the up-state was variable. On average across animal studies, it was located in middle and deep layers (most probably layer III-V) in natural sleep, whereas in superficial layers (most probably layer II-III) under urethane anesthesia.

Sanchez-Vives et al. analysed the fine scale laminar structure of neuronal activity, revealing that firing during the up-state in slice preparations is the earliest in the infragranular layers and spread towards the superficial layers with a long ~100ms inter-laminar delay. In intact animals the up-state onset related initial firing, intracellular

membrane potential and LFP changes could be detected in any layer in a probabilistic manner, with a short inter-laminar delay (~10ms), however, on average, the earliest activity was found in the infragranular layers.

Although the cellular and synaptic/trans-membrane mechanisms of slow waves are under intense investigation in animals, these mechanisms have not previously been studied in humans. Presurgical diagnostic procedures in epilepsy may allow the experimenter to open an invasive window on the brain and record local field and action potentials to investigate the fine scale generators of electrical brain oscillations.

Objectives

Previous studies of SWA in humans have been limited to macroelectrode recordings that superimpose activity from several cm^2 of cortex. These recordings are ambiguous as to the circuits involved, are not sensitive to neuronal firing, and do not distinguish between excitatory and inhibitory mechanisms. We used laminar multichannel microelectrode array recordings to estimate neuronal firing and synaptic/trans-membrane currents in different cortical layers. Since cortical neuronal populations and synaptic inputs are organized into distinct layers, these recordings allowed us to resolve the cortical generators underlying SWA in humans.

Methods

Five patients with intractable epilepsy underwent chronic clinical subdural electrocorticography (ECoG) grid and strip electrode implantation as a standard procedure for localization of the seizure focus and eloquent areas. Fully informed consent was obtained from each subject under the auspices of the Hungarian Medical Scientific Council and local ethical committee; National Institute of Neuroscience, Budapest, Hungary according to the World Medical Association Declaration of Helsinki. In addition to the surface electrodes, a 24 contact experimental laminar multichannel microelectrode array (ME) was implanted perpendicular to the cortical surface, underneath the clinical grids. The contacts were spaced evenly providing LFP recordings from layer I to layer VI. The location and duration of the clinical electrode implantation were determined entirely by clinical considerations, the ME was placed in cortex that was likely to be removed at the definitive surgery.

The positions of the electrodes were confirmed by intraoperative navigation, co-localization of intraoperative photographs, pre- and postoperative MR scans and 3D MR reconstructions. The brain tissue containing the electrode track in Patients 4 and 5 was removed en-bloc for further anatomical analysis. Layers of the neocortex were outlined using NeuN, calretinin (CR), SMI-32, and glial fibrillar acidic protein (GFAP) stains.

After electrode placement, a video-EEG observation took place in order to localize the seizure focus. Spatial LFP gradient (LFPg), the voltage difference between consecutive laminar electrode contacts was split to EEG range (0.1-300 Hz) and single (SUA), multiple unit activity (MUA) frequency range (300-5000 Hz) by analogue band-pass filtering. EEG range signal was sampled at 2 kHz / 16 bit; MUA range was sampled at 20 kHz / 12 bit.

We have analyzed the LFPg, MUA, SUA and ECoG data acquired from each patient. Sleep staging was performed based on readings of the available scalp EEG and ECoG electrodes by expert neurologists. In this study, we have analyzed electrophysiological data obtained only from the deepest stage of NREM sleep (N3, or SWS). Data containing interictal spikes (within 1 min) and seizures (within 60 min) were excluded from the study to avoid epileptic contamination.

In addition to spectral and autocorrelation analyses, SWA cycle detection was based on phase and amplitude information, extracted from the narrow-band filtered (0.3-3 Hz, 24 dB/octave, zero phase shift) layer II LFPg and ECoG data. Instantaneous phase of the filtered signal was calculated by the Hilbert transformation. In addition to phase constraints, valid SWA cycles had to fulfil amplitude criteria. The SWA detection algorithm parameters were tuned and carefully validated by expert electroencephalographers.

To quantify and compare SWA parameters with other studies, the frequency of SWA occurrence (detected valid cycles per minute), the interdetection interval histogram and the cycle length histogram

were calculated. The single sweep and averaged time-frequency content of the SWA signal was also computed using wavelet transforms. In addition, we attempted to describe the laminar distribution of the SWA in more detail using the LFPg FFT power spectrum depth profile, the pairwise linear coherence between each LFPg trace in the SWA (0.3-3 Hz) frequency range, and the depth profile of the LFPg autocorrelation.

CSD analysis identifies synaptic/trans-membrane generators of LFP in laminated neural structures. The negative of the second spatial derivative of the LFP closely approximates the macroscopic current density over unity cell membrane area. Since LFPg is the first spatial derivative of LFP, one additional spatial derivation yielded the CSD for the EEG range (0.1-300 Hz) data. High spatial frequency noise and boundary effects were reduced by Hamming-window smoothing and interpolation.

For statistical analysis, ANOVA with Tukey's HSD (honestly significant difference) test were applied to the normalized values (LFPg and CSD: between -1 and +1; MUA, gamma band LFPg and CSD: between 0 and 1).

In Patients 4 and 5 (with available histology), the averaged, normalized CR+ cell density and averaged, normalized electrophysiology depth profiles (consecutive values at each cortical depth) were constructed. The normalized cell density and electrophysiology measures were compared using the Pearson r correlation method with $p<0.01$ significance level criterion.

A continuous estimate of population neuronal firing rate was calculated from the MUA range (300-5000 Hz) data. Putative single units were analyzed by conventional threshold detection and clustering methods. A spike train was determined as a burst, if at least three consecutive spikes occurred within a maximum 20 ms long interval, which was preceded and followed by at least 20 ms long intervals with neuronal silence.

Phase dependence of single cell firing rate was computed for 30° phase bins; the total number of firing in a given bin was divided by the total time that the cortex spent in that phase bin (thus producing a phase histogram). The Rayleigh test ($p<0.01$) was used to judge if the resulting circular distribution was significantly different from the uniform distribution.

Results

I. Human slow wave activity reflects a rhytmic oscillation in the extracellular local field potential: the surface positive half-wave corresponds to the depolarized up-state with increased cell firing and the surface negative half-wave corresponds to the hyperpolarized down-state with neuronal silence.

Automatic SWA cycle detection was applied to determine the phase of SO. It revealed on average 20 SWA cycles (*mean*=20 1/min, *range*=12-26 1/min, *SD*=7 1/min) per minute. Cycle length peaked on

average at 0.8 sec (*mean*=0.8 sec, *range*=0.6-1.4 sec, *SD*=0.3 sec). Interdetection interval peaked on average at 1.1 sec (*mean*=1.1 sec, *range*=0.8-1.2 sec, *SD*=0.4 sec), all comparable to healthy subjects (Figure 1).

The LFP during the SO was positive in the superficial layers during the up-state and negative during the down-state. This polarity was reversed in the middle layers, causing negative field potentials in the deep layers during the up-state, and positive LFP during the down-state. Neuron activity was increased during up-states and virtually absent during down-states (Figure 2B).

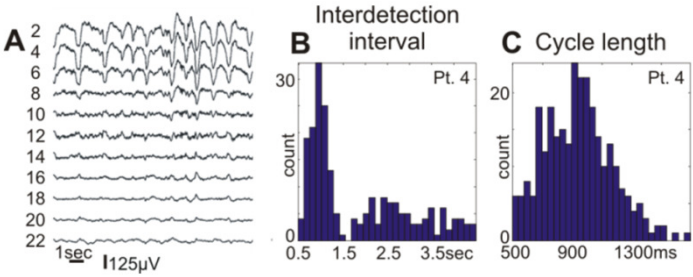

Figure 1. (A) Representative example of LFPg recordings during SWS in patient 4. Every second recording channel is shown. (B) Representative examples of interdetection interval histogram (y-axis: counts, x-axis: time between up-state detections, 166 ms bin) and (C) cycle length histogram (y-axis: counts, x-axis: valid cycle lengths, 33 ms bin) in Patient 4.

II. *The increase in wideband (0.3-200 Hz) spectral power, multiunit and single unit activity, and inward transmembrane currents, associated with the up-state; and the decrease in spectral power, unit activity, and outward transmembrane currents, associated with the down-state, are mainly localized to the supragranular layers.*

To estimate the laminar contribution of various activities, ME channels were assigned into six putative layers (I-VI) based on the histological findings when available, and cortical depth when not. This analysis revealed substantial concentration of the 0.3-3 Hz band LFPg FFT power within layers I-III in each patient, indicating strong supragranular synaptic/trans-membrane activity. The SWA shape similarities between electrode contacts were significantly greater in supragranular versus infragranular layers in each patient, (0.634 versus 0.423, grand average pairwise coherence, Kruskal-Wallis ANOVA, $p<0.01$), while autocorrelation profiles revealed a more precisely paced rhythm supragranularly in each patient.

Several measurements, both in individual patients and in grand averages, reflecting different aspects of population synaptic/trans-membrane and firing activity, were maximal in supragranular layers at the up-state peak. Normalized, grand average depth profiles of LFPg were marked by maximally positive deflections in layers I-III, inverting in layers V-VI into a small negativity. MUA was also maximal in layer III. The CSD depth profile at the peak of the SWA up-state showed a maximal source (outward current) in layer I and maximal sink (inward current) in layers II-III, only very small CSD deflections were observed infragranularly. Significant increases (bootstrap analysis, $p<0.01$) in LFPg spectral power were detected in all layers at 10-100 Hz frequencies during up-states. Gamma power of LFPg and CSD was maximal in layer III (Figure 2).

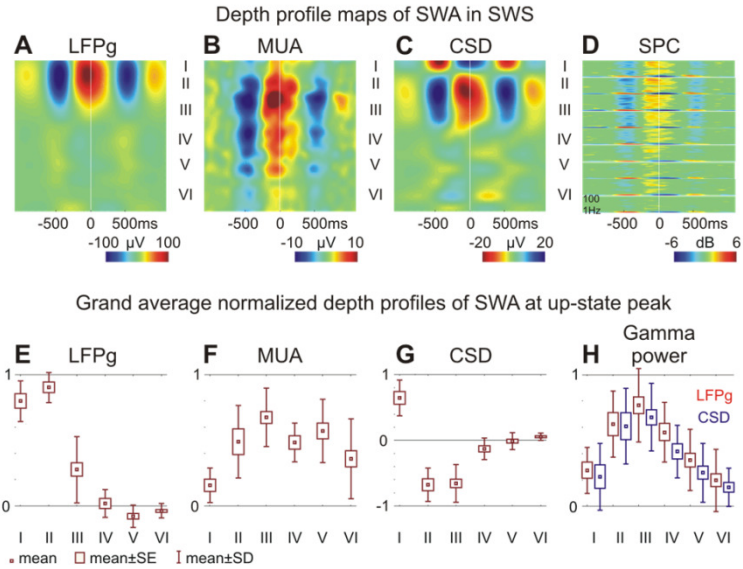

Figure 2. Role of supragranular layers in SWA generation. Representative depth profile map examples from Patient 4 (A-D) and grand averages of all patients (E-H). (A) LFPg, (B) MUA, and (C) CSD depth profile maps. X-axis: time, Y-axis: cortical depth, with corresponding laminarization, Z-axis: colour coded amplitude of LFPg, MUA and CSD units. Positive values are red, negative are blue, except for CSD, where sink is depicted in red and source in blue. (D) LFPg spectrograms from nine representative channels in layers I-VI. X-axis: time, Y-axis: frequency, Z-axis: colour coded averaged relative spectral power in dB. Box-whisker plots of (E) LFPg, (F) MUA, (G) CSD, (H) LFPg (red) and CSD (blue) gamma power (30-150Hz); normalized grand average of all patients at the peak of the up-state in each layer. Mean: small box, standard error (SE): large box, standard deviation (SD): whisker.

Calretinin positive cell density depth profiles were calculated in two patients and correlated with the depth profile at up-state peak of LFPg, CSD, MUA, LFPg and CSD gamma power (Figure 3). CR+ cell density between Patient 4 and 5 showed high similarity (r=0.95, p<0.01). The highest positive correlation was found between CR+ cell density and CSD gamma power (r=0.85, p<0.01).

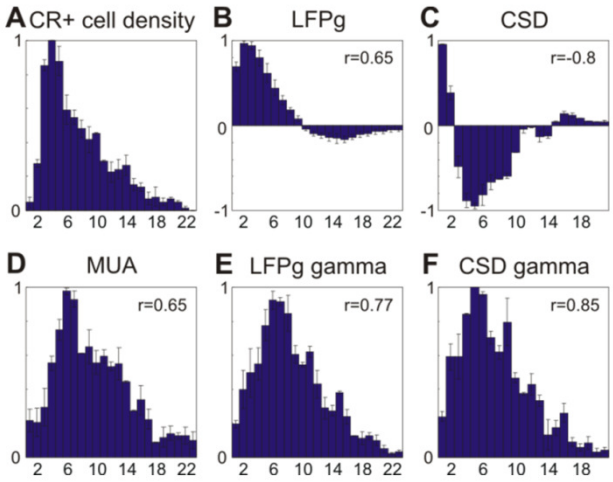

Figure 3. Depth profiles of CR+ cell density and SWA. (A) Averaged normalized CR+ cell density profile of Patients 4 and 5, whiskers represent standard errors. (B) LFPg, (C) CSD, (D) MUA, (E) LFPg gamma power and (F) CSD gamma power of averaged normalized depth profile of up-state in Patients 4 and 5 with standard error (whisker). Number in the upper right corner indicates the Pearson r correlation between CR+ density and (B-F).

III. Action potentials at up-state onset are synchronized within ±10 ms across all cortical layers, suggesting that any layer could initiate firing.

The time courses of MUA were examined to determine if one layer may lead others. It was shown in ferret slices that layer V MUA consistently led layers II-III by an average of over 100 ms. In our study, the up-state associated MUA peak-locked averages indicated no evident timing difference in any of the patients, between layers III and V, regardless of whether peak alignment was based on layer III or layer V activity (Figure 4C).

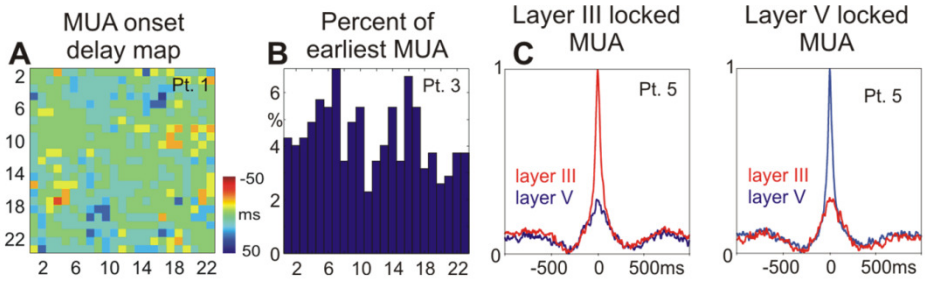

Figure 4. Simultaneity of MUA response in supra- and infragranular layers. (A) MUA cross-correlation peak latencies (X-axis versus Y-axis) between each pair of channels in Patient 1. Positive latencies (red) indicate that X channel leads over Y channel, while negative latencies (blue) represent lagging. (B) Percentage of a given MUA channel showing the earliest firing at up-state onset, representative data from Patient 3. (C) MUA from layers III (red trace) and V (blue) are shown when aligned and averaged on the up-state associated MUA peak detected in layer III and in layer V. There is no visible MUA delay between layers III and V regardless of which layer is used for time locking.

To further characterize the MUA timing between different layers, it was cross-correlated (3 *SD* threshold, 10 ms bin size) between each pair of channels, within 200ms of every up-state onset. In agreement with animal studies, delay maps and histograms indicated a short inter-laminar MUA timing difference at up-state onset; most of the delays were within the ±10 ms bin (Figure 4A). We also calculated how often (in percentage of all sweeps) any given MUA channel shows the earliest firing at up-state onset. In all patients (where MUA was available), the initial firing was quite uniformly distributed across cortical depths (Figure 4B). Unlike in a ferret in vitro study, we found no evidence for long (~100 ms) lead or lag times between different layers.

IV. The laminar mechanisms generating slow oscillation are similar within frequency bands 0.6-2 Hz.

Separate averages of different SWA cycle lengths corresponding to appropriate (0.6-0.8 Hz, 0.8-1 Hz, 1-1.3 Hz and 1.3-2 Hz) oscillation frequencies also yielded qualitatively similar LFPg, spectral LFPg, MUA and CSD distribution (Figure 5). We have found no statistically significant differences in any layers (ANOVA, Tukey's HSD post-hoc test, $p>0.3$) in the CSD or MUA at the peak of the up-state between any of the four frequency bands indicating similar cortical generator mechanisms above (up to 2 Hz) and below 1 Hz (down to 0.6 Hz).

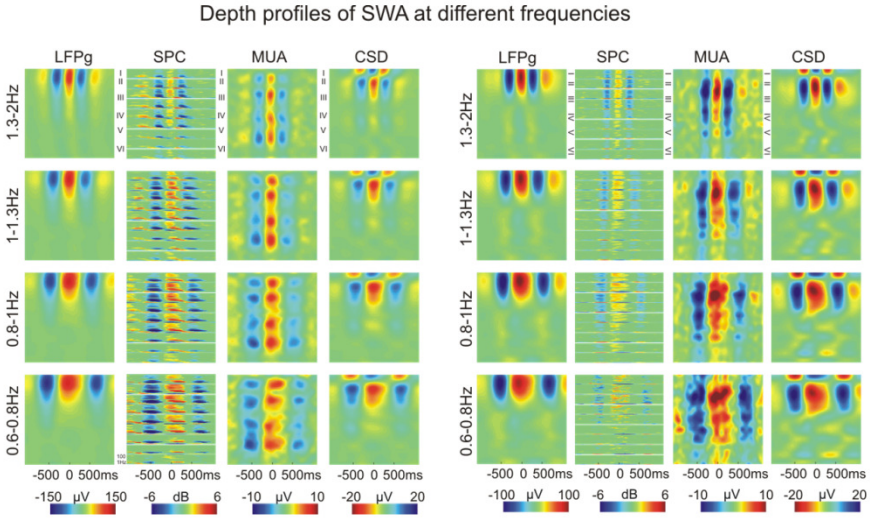

Figure 5. Depth profiles at different SWA frequencies. Up-state locked averages of LFPg, LFPg spectrogram, MUA and CSD in Patient 3 and 4 at four different SWA frequencies. Frequencies 1.3-2Hz, correspond to a cycle length of: 500-750 ms; 1-1.3 Hz to 750-1000 ms; 0.8-1 Hz to 1000-1250 ms; and 0.6-0.8 Hz to 1250-1500 ms. Roman numerals mark putative cortical

layers. Colour calibrations are on the bottom. CSD sink is depicted in red, source in blue. Each spectrogram (SPC) window shows the spectral content (Z-axis, colour coded) versus time (X-axis) of a representative LFPg channel from a given layer from 1-100 Hz (Y-axis), measures are expressed in dB relative to a distant baseline (-2500 to -1500 ms).

V. Neuronal firing in the up-state is sparse compared to extracellular recordings in animals.

Recordings from three patients yielded good quality single unit activity. Epochs (~1000 sec) showing the largest SWA detection frequencies were selected for analysis from the first sleep cycle. Overall 33 single units were clustered (9, 12 and 12 from Patients 1, 4 and 5) with mean firing rate of 0.66 Hz (*range*=0.12-2.0 Hz, *SD*=0.48) and mean burst frequency of 3.1 1/minute (*range*=0-14 1/minute, *SD*=3.6). Both the average firing rate and the spontaneous burst rate were well below the reported epileptic threshold found in cortical and hippocampal structures.

Nearly all cells (31 of 33) showed significantly non-uniform spiking over the SWA cycle (Rayleigh test, $p<0.01$), with peak up-state firing rate mean of 1.63 Hz (*range*=0.45-4.6 Hz, *SD*=0.96). We found no significant differences between patients in mean firing rates (Kruskal-Wallis ANOVA, $p>0.2$), indicating homogeneous distribution. Although mean firing rates grouped by supra- versus infragranular layers showed no significant differences ($p>0.1$), supragranular peak up-state firing rates were significantly higher (2.2 Hz versus 1.2 Hz, Kruskal-Wallis ANOVA, $p<0.01$) than the same measure for

infragranular layers. We found the proportion of firing cells and the rate at which they fire in any given up-state remarkably low. On average, only 27% of the clustered cells were active (firing at least one spike) during any given up-state (20%, 25% and 36% in each patient). Moreover, on average, each neuron fired only 0.32 spikes per up-state (0.44, 0.2 and 0.32 in each patient). As an example, out of the 12 clustered neurons in Patient 4, the most probable number of active cells in a given up-state was 2, and the most probable number of overall spikes the 12 cells fired within a given up-state was also 2 (Figure 6). These data illustrate sparse firing in up-states, only a small fraction of the clustered cells fire and these cells together generate only a few action potentials.

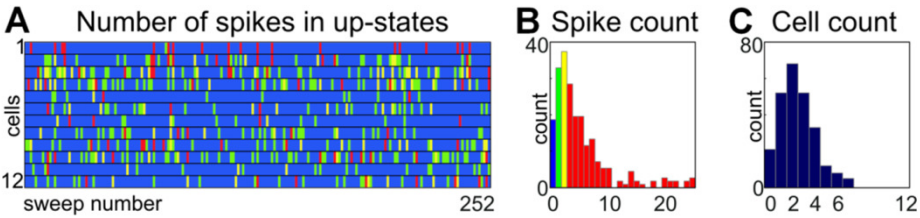

Figure 6. Single unit data from Patients 4 indicating sparse firing in up-states. (A) Colour raster plot illustrates the firing of clustered neurons in up-states. Columns represent individual SWA cycles (n=252), rows represent clustered neurons (cell 1-12 in Patient 4), colour represents the firing of a given cell. Blue: no firing in the given up-state for the given cell, green: one, yellow: two, red: three or more action potentials. (B) Histogram of the total number of fired action potentials (spike number count) from all clustered cells during a given up-state (X-axis: total number of action potentials fired by all cells, Y-axis: number of up-states with that number of action potentials, count). (C) Histogram of the number of active clustered cells (active cell count) during the up-states (X-axis: number of cells that fired at least one action potential, Y-axis: number of up-states, count).

Discussion

Our results establish a close similarity between the human SWA and the animal SO at the level of field potential, cellular firing activity and spectral measurements, but also reveal a number of novel, unexpected findings. Consistent with prior studies in animals, we have shown in humans that the up-state was associated with increased firing and elevated spindle, alpha, beta, gamma and ripple power during the surface positive LFP half-wave, while the down-state was characterized by the widespread surface negative LFP half-wave with decreased firing, and oscillatory activity. Differences from prior studies were found in the laminar distribution of the up-state, the earliest neuronal activity at the onset of the up-state, average firing rates, and the consistency of generators for oscillations above versus below one Hertz.

The strong supragranular oscillatory activity in sleep may be beneficial for the local, higher order processing of sensory experience and perhaps memory consolidation, since these layers are interconnected by dense cortico-cortical projections forming fine-scale functional networks to perform integrative functions. The weaker infragranular activity may reflect the relatively suppressed cortical executive, output functions, which may prevent effective connectivity between distant cortical areas from developing in SWS.

The apparently lower firing rates of human cortical neurons during up-states may also reflect an adaptation to prevent runaway excitation of our larger and more densely interconnected neocortex, or it

may better support the sparse representation of our extensive long term memories

These contrasts could reflect cortical cytoarchitectonic differences or they could be due to the circumstances of the recordings, including natural sleep versus different types of anaesthesia, or in vivo versus in vitro preparations. They could also be due to epileptic pathology or to phylogenetic differences.

Publications

'Laminar analysis of the slow wave activity in humans',
Csercsa R., Dombovári B., Fabó D., Wittner L., Erőss L., Entz L., Sólyom A., Rásonyi Gy., Szűcs A., Kelemen A., Jakus R., Juhos V., Grand L., Magony A., Halász P., Freund T. F., Maglóczky Zs., S. S. Cash, Papp L., Karmos Gy., E. Halgren, Ulbert I.,
Brain, 133(9):2814-29., 2010., IF: 9.490

'The human K-complex represents an isolated cortical down-state',
S. S. Cash, E. Halgren, N. Dehghani, A. Rossetti, T. Thesen, C. Wang, O. Devinsky, R. Kuzniecky, W. Doyle, J. R. Madsen, E. Bromfield, Erőss L., Halász P., Karmos Gy., **Csercsa R.**, Wittner L., Ulbert I.,
Science, 324(5930):1084-7., 2009., IF: 29.747

'Short and long term biocompatibility of NeuroProbes silicon probes',
Grand L., Wittner L., S. Herwik, E. Göthelid, P. Ruther, S. Oscarsson, H. Neves, Dombovári B., **Csercsa R.**, Karmos G., Ulbert I.,
J Neurosci Methods, 189(2):216-29., 2009., IF: 2.295

'Control and data acquisition software for high-density CMOS-based microprobe arrays implementing electronic depth control',
K. Seidl, T. Torfs, P. A. De Mazière, G. Van Dijck, **Csercsa R.**, Dombovári B., Y. Nurcahyo, H. Ramirez, M. M. Van Hulle, G. A. Orban, O. Paul, Ulbert I., H. Neves, P. Ruther,
Biomedizinische Technik, 55(3):183-91., 2009., IF: 0.525